Journal of Colloid And Interface Science

Triple-emission N, B co-doped carbon quantum dots from lignin: Highly fluorescent sensing platform for detection of Cr6+

--Manuscript Draft--

Manuscript Number:	
Article Type:	Full length article
Section/Category:	A. Colloidal Materials and Nanomaterials
Keywords:	Lignin; Carbon quantum dots; N, B co-Doped; Triple channel; Sensing Cr6+
Corresponding Author:	Dekui Shen Southeast University Nanjing, CHINA
First Author:	Lingli Zhu
Order of Authors:	Lingli Zhu
	Dekui Shen
	Kai Hong Luo
Abstract:	Considering that Cr6+ with high toxicity poses huge threat to human health and ecological environment, the construction of a rapid and accurate fluorescence sensing platform is of great significance to detect the toxic substance. The N,B-CQDs from lignin waste are synthesized as fluorescent sensor for Cr6+ detection. The synthetic processes involve the acid hydrolysis step followed by the hydrothermal treatment. Lignin is firstly depolymerized by cleaving ether bonds under the action of acid, and N,B-CQDs are consequently formed by the aromatic re-fusion of lignin fragments in the carbonation process. The resultant N,B-CQDs show triple fluorescent emission of purple, blue and green color under the excitation of 300, 330, and 490 nm. The N,B-CQDs can be applied for the triple-channel detection of Cr6+, exhibiting highly sensitive and selective fluorescence quenching in the presence of Cr6+ with good linearity (R2≤0.996) and very low limit of detection as 0.054, 0.049 and 0.077 μM for Ex 300, 330 and 490 nm channel, respectively. The utilization of renewable lignin highlights the green, cheap and large-scale production of CQDs based fluorescent sensors and opens a new avenue for the rapid and accurate detection of Cr6+ through multichannel sensing platform.
Suggested Reviewers:	Mingyue Ding Wuhan University dingmy@whu.edu.cn
	Haiping Yang Huazhong University of Science and Technology yhping2002@163.com
	Chunfei Wu Queen's University Belfast c.wu@hull.ac.uk
	Sai Gu University of Surrey sai.gu@surrey.ac.uk
	Dan Shan Nanjing University of Science and Technology Danshan@njust.edu.cn

Cover letter

Dear Editor,

I, on behalf of all authors, would submit the manuscript entitled "Triple-emission N, B co-doped carbon quantum dots from lignin: Highly fluorescent sensing platform for detection of Cr^{6+}" to the ***Journal of Colloid and Interface Science***.

Cr^{6+} with high toxicity poses huge threat to human health and ecological environment, the construction of a rapid and accurate fluorescence sensing platform is of great significance. CQDs based fluorescent sensors show promising potentials for the detection of Cr^{6+} due to their nontoxicity, rapid response and adjustable fluorescence characteristics. Among them, biomass-derived CQDs with low cost, renewability and environmentally friendly are expected to realize green and mass production of fluorescent sensors. In this work, N, B-CQDs from lignin waste are synthesized as fluorescent sensor for Cr^{6+} detection via a facile two-step method. The resultant N, B-CQDs exhibit triple fluorescent emission under different excitations and their formation mechanism is also excavated. N, B-CQDs are employed as fluorescent sensors for the triple-channel detection of Cr^{6+} with superior sensitivity and selectivity. This work hopes to offer a new insight on in-depth understanding of formation mechanism for lignin-derived N, B-CQDs and open new avenue for the rapid and accurate detection of Cr^{6+} through multichannel sensing platform.

I sincerely appreciate you for reviewing the manuscript and considering the publication of this review. Look forward to your positive feedback. Thanks a lot!

Prof. Dekui Shen

Key Laboratory of Thermal Conversion and Control, Ministry of China

School of Energy and Environment, Southeast University

E-mail: 101011398@seu.edu.cn

3: Graphical Abstract

Graphic abstract

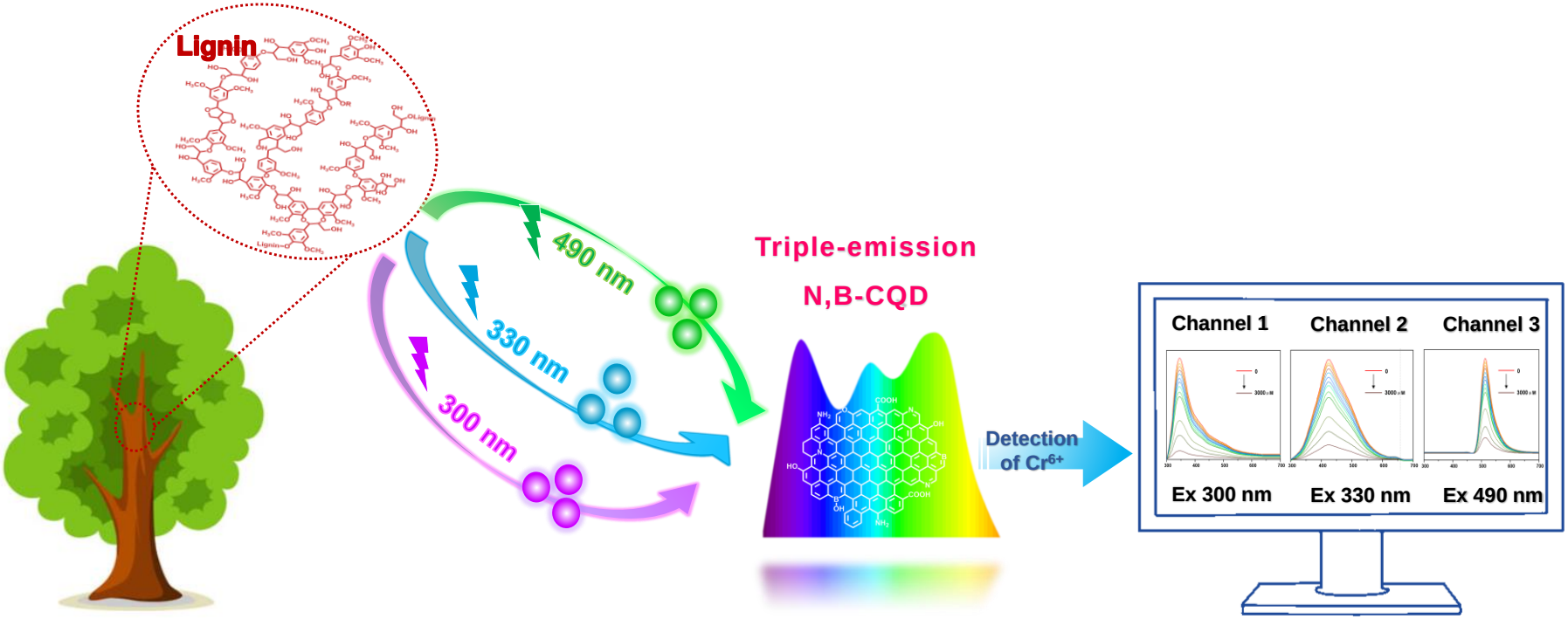

Triple-emission N, B co-doped carbon quantum dots from lignin: Highly fluorescent sensing platform for detection of Cr^{6+}

Lingli Zhu[a], Dekui Shen[a,*] Kai Hong Luo[b]

[a] Key Laboratory of Energy Thermal Conversion and Control of Ministry of Education, School of Energy and Environment, Southeast University, Nanjing 210096, PR China.

[b] Department of Mechanical Engineering, University College London, London WC1E7JE, U.K.

E-mail address: 101011398@seu.edu.cn (D. Shen)

ABSTRACT: Considering that Cr^{6+} with high toxicity poses huge threat to human health and ecological environment, the construction of a rapid and accurate fluorescence sensing platform is of great significance to detect the toxic substance. The N,B-CQDs from lignin waste are synthesized as fluorescent sensor for Cr^{6+} detection. The synthetic processes involve the acid hydrolysis step followed by the hydrothermal treatment. Lignin is firstly depolymerized by cleaving ether bonds under the action of acid, and N,B-CQDs are consequently formed by the aromatic re-fusion of lignin fragments in the carbonation process. The resultant N,B-CQDs show triple fluorescent emission of purple, blue and green color under the excitation of 300, 330, and 490 nm. The N,B-CQDs can be applied for the triple-channel detection of Cr^{6+}, exhibiting highly sensitive and selective fluorescence quenching in the presence of Cr^{6+} with good linearity ($R^2 \leq 0.996$) and very low limit of detection as 0.054, 0.049 and 0.077 μM for Ex 300, 330 and 490 nm channel, respectively. The utilization of renewable lignin highlights the green, cheap and large-scale production of

CQDs based fluorescent sensors and opens a new avenue for the rapid and accurate detection of Cr^{6+} through multichannel sensing platform.

Keywords: Lignin; Carbon quantum dots; N, B co-Doped; Triple channel; Sensing Cr^{6+}

1. Introduction

Chromium is widely distributed in the ecosystem in the form of Cr^{3+} and Cr^{6+} [1]. Cr^{3+} is considered as an indispensable trace element in the human body, while Cr^{6+} is extremely highly toxic heavy metal contaminant, which is ca. 100 times more toxic than Cr^{3+} [2]. Massive Cr^{6+} has been discharged into the biological environment from industrial effluents and waste residue produced by stainless steel manufacturing, ore smelting, dyeing, leather tanning, metal electroplating, etc. [3, 4]. Excessive Cr^{6+} is carcinogenic and mutagenic to respiratory tract, internal organs and nerve tissue owing to its high oxidation potential and super ability to penetrate biomembranes, posing a great threat to the environment and human health [5-7]. The maximum allowable limit of Cr^{6+} in drinking water is 1.92 μM as stipulated by the United States Environmental Protection Agency (USEPA), 0.962 μM by the World Health Organization (WHO), and in aquatic products is 2 mg/kg by the National Food Safety Standard of China (GB, 2762–2012) [8, 9]. Thus, the development of effective detection technology for Cr^{6+} is a top priority to ensure the safety of food and drinking water sources.

Currently, traditional detection techniques for Cr^{6+} include atomic absorption spectrometry (AAS), atomic emission spectrometry (AES), inductively coupled plasma-mass spectrometry (ICP-MS), and electrochemical detection [10-12]. However, these methods have several drawbacks of large or costly equipment, time-consuming preprocessing, complex operation and tedious analysis, which limit the large-scale rapid detection of Cr^{6+} [13]. In

comparison, the fluorescent detection method for Cr^{6+} can overcome these issues for its simple, fast, real-time and intuitive merits [14-16]. Among them, carbon quantum dots (CQDs) based fluorescent detection method for Cr^{6+} shows great promise due to its nontoxicity, good water solubility, rapid response as well as adjustable fluorescence characteristics [16]. Wang et al. [6] synthesized bright blue fluorescent N,S co-doped CQDs using citric acid monohydrate and thiosemicarbazide as raw materials via hydrothermal reaction. The N, S-CQDs based sensors not only exhibited sensitive fluorescence response for Cr^{6+} ions with the LOD of 0.33 μM, but also for toluene in ethanol solution with the LOD of 0.03 μM. Similarly, the N, S-CQDs based fluorescent sensors were obtained by Ji et al. [12] from the rapid stirring of L-cysteine and urea, which showed the LOD as low as 0.02 μM for Cr^{6+} detection along with 0.28 μM for ascorbic acid detection. Zheng and co-workers [17] designed controllable functionalization of N-CQDs from carbon rods through electrochemical method followed by the solvothermal treatment with ammonia, N,N-Dimethylformamide or polyethylene glycol, respectively. The resultant three kinds N-CQDs were as fluorescent sensors for independent Cr^{6+}, Fe^{3+} and Cu^{2+} ions detection. Nevertheless, the CQD-based Cr^{6+} sensors are still largely underdeveloped with the bottleneck in selectivity and reproducibility. It might be attributed to their strong affinity for Fe^{3+} or other substances by naturally abundant phenolic hydroxyl attached on the surface of CQDs [18]. In addition, using toxic organic small molecules as raw materials for CQDs production is bound to add the risk to the environment and human health. Accordingly, there is an urgent need for the development of superior CQDs based fluorescent sensors with higher selectivity, greater practicability and more environmental friendliness.

In this work, the green synthesis of N,B co-doped CQDs from sustainable lignin via a mild two-step approach is proposed for the fluorescent detection of Cr^{6+}. The physicochemical properties of N,B-CQDs are comprehensively characterized and the formation mechanism is also excavated. Utilizing its unique triple emission property, a highly fluorescent tri-channel sensing platform has established for rapid and accurate detection of Cr^{6+} ions. The lignin derived CQDs using as fluorescent sensors offer a green, low-cost, and available strategy for the sensitive detection of Cr^{6+} in a large scale.

2. Experimental section

2.1 Reagents and materials

Alkali lignin with 4% sulfur was acquired from Sigma-Aldrich (Shanghai, China). 3-Aminophenylboronic acid (≥98%) was purchased from Aladdin (Shanghai, China). Other chemicals, including $NaCl_2$, NaF, Na_2S, $NaNO_3$, Na_2SO_3, Na_2SO_4, NaH_2PO_2, KCl, $NiCl_2.6H_2O$, $MgCl_2.6H_2O$, $CuCl_2.H_2O$, $CaCl_2$, $ZnCl_2$, $FeCl_3.6H_2O$, and K_2CrO_4 were purchased from Macklin (Shanghai, China). Deionized (DI) water was used throughout this experiment. The dialysis bags with retained molecular weight of 1000 Da were provided by Viskase (USA). The microporous filter membranes of aqueous system with the diameter of 1.0 and 0.10 μm were obtained by Jinteng (Tianjin, China). All chemicals were used without any further purification.

2.2 Preparation of N,B-CQDs

In a typical two-step synthetic route of N,B-CQDs, 0.3 g of 3-aminophenylboronic acid was added into 30 mL of DI water, and 0.3 g of AL was manually mixed under constant

stirring. The mixed solution was then heated at 90 ℃ for 1 h in water bath with constant stirring (350 rpm). The solution after the reaction was vacuum filtered by a PTFE microporous membrane (1.0 μm). The lignin nanoparticles (LNPs) can be obtained by directly freeze-drying the filtrate. Subsequently, the obtained filtrate was transferred into a Teflon-lined autoclave (50 mL) and kept at a certain temperature for 12 h. The resultant CQDs were cooled to room temperature and further filtered out by a microporous filter membrane (0.10 μm). The remaining filtrate was dialyzed in a dialysis bag against DI water for 2 days. The as-dialyzed CQDs aqueous solution was freeze-dried under -60 ℃ for 2 days and the powders were finally collected for characterization and property measurements. The effect of different temperature of 120, 150, 180, 200 and 220 ℃ on the lignin-derived CQDs has been investigated. The resultant N,B-CQDs are named as CQDs-120, CQDs-150, CQDs-180, CQDs-200, and CQDs-220, respectively.

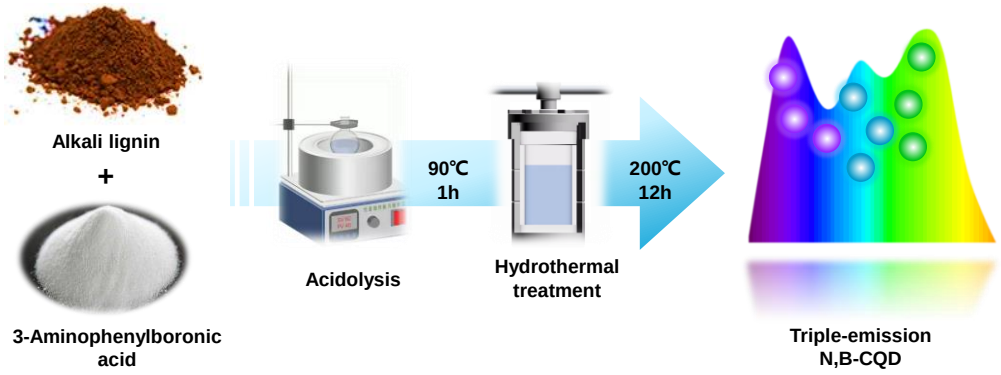

Scheme 1. Illustration for the synthetic route of triple-emission N, B-CQDs.

2.3 Characterization

The detailed morphology was observed using a high-resolution transmission electron microscope (HR-TEM, Tecnai G2 F20, FEI, USA). The graphitized structure was recorded by a Micro-Raman spectrometer with InGaN laser excitation at 532 nm (DXR 2xi, ThermoFisher,

USA). The chemical composition was characterized by a Fourier transform infrared spectrometer (FT-IR, Nicolet Is5, ThermoFisher, USA) and an X-ray photoelectron spectrometer (XPS, K-Alpha, ThermoFisher, USA). The molecular weight was obtained by a matrix-assisted laser desorption/ ionization time of flight mass spectrometer (MALDI-TOF MS, ultrafleXtreme, Bruker, Germany). The ^{13}C-^{1}H chemical environment was measured by the two-dimensional heteronuclear singular quantum correlation nuclear magnetic resonance spectrometer (2D-HSQC NMR, Avance III 600 MHz, Bruker, Germany) with the dispersant of dimethyl sulfoxide-d6 (DMSO) for AL and deuterium oxide (D_2O) for LNP and CQD. The optical properties were measured by an ultraviolet−visible spectrophotometer (UV-vis, UV-5200, Yuanxi, China) and a fluorescence spectrophotometer (Cary Eclipse, Agilent, USA). The time-resolved PL spectra were acquired from a steady/transient state fluorescence spectrophotometer (TRPL, FLS1000, Edinburgh, UK) equipped with an integrating sphere to evaluate the absolute QY of CQDs. The obtained lifetime decay curves were fitted using a multi-exponential function R(t) (eq. (1)) and the average lifetime (τ_{avg}) was calculated according to eq. (2).

$$R(\mathrm{t}) = A_1 e^{(-t/\tau_1)} + A_2 e^{(-t/\tau_2)} \ldots\ldots + A_n e^{(-t/\tau_n)} \quad (1)$$

$$\tau_{avg} = (A_1\tau_1^2 + A_2\tau_2^2 + \cdots .. A_n\tau_n^2) \,/\, (A_1\tau_1 + A_2\tau_2 \ldots\ldots .. + A_n\tau_n) \quad (2)$$

Where τ_1, τ_2 ..... τ_n represent fluorescence decay lifetimes and A_1, A_2 ..... A_n represent pre-exponential factors of τ_1, τ_2 ..... τ_n, respectively.

2.4 Fluorescent detection of Cr(VI)

The fluorescent detection of a series of interfering ions (Cl^-, NO_3^-, F^-, S^{2-}, SO_3^{2-}, SO_4^{2-}, $H_2PO_2^-$, Na^+, Ni^{2+}, Mg^{2+}, Cu^{2+}, Ca^{2+}, K^+, Zn^{2+}, Fe^{3+}, and Cr^{6+}) was performed at room

temperature. 3 mg of N,B-CQD powders were added into 1 L of ion solutions in a concentration of 600 μM and rested for 30 min. Then their PL emission spectra were recorded at 300, 330 and 490 nm excitation, respectively. In addition, different concentrations of Cr^{6+} including 0, 20, 40, 60, 80, 100, 200, 400, 600, 800, 1000, 1500, 2000 and 3000 μM were added into N,B-CDs aqueous solution, respectively. The corresponding PL emission spectra of these mixtures were measured at 300, 330 and 490 nm excitation, respectively. The theoretical limit of detection (LOD) was calculated according to eq. (3):

$$\mathrm{LOD} = 3\partial/K \quad (3)$$

Where 3 refers to the signal-to-noise ratio; σ refers to the standard deviation of the blank signal; *K* refers to the slope of the linearly concentration-dependent response.

3. Results and discussion

3.1 Morphological structure of N, B-CQDs

The lignin-derived N,B-CQDs are obtained through a mild two-step route involving acid hydrolysis followed by hydrothermal treatment. The hydrothermal temperatures ranging from 120 to 220 ℃ are optimized based on the fluorescence QYs of N,B-CQDs at different excitation wavelengths. According to Fig.S1, N, B-CQDs synthesized at 200 ℃ shows the highest QYs under 300, 330 and 490 nm excitation, respectively, which is selected to be further characterized and investigated. The micromorphology of N, B-CQDs can be observed by TEM as shown in Fig.1, which are well-dispersed quasi-spherical nanoparticles with an average diameter of 3.82 nm. The HR-TEM images clearly exhibit one kind of lattice fringe with interplanar spacing of 0.34 nm, which represents the (002) crystal plane of graphite [19,

20]. The graphitization of AL, LNP and CQDs is recorded by Raman spectra (Fig. 2a). There are two apparent peaks at 1356 cm^{-1} (D band) and 1572 cm^{-1} (G band), corresponding to the vibrations of disordered sp^3 carbon and graphitized sp^2 carbon [21]. The relative intensities (I_D/I_G) of AL, LNP and CQDs, an indicator of the defect density in their structure [22, 23], are 1.55, 2.38, and 1.05, respectively. It indicates that more structural defects are introduced in LNP after the acidolysis of AL while more graphitized structure in CQD after the hydrothermal reaction.

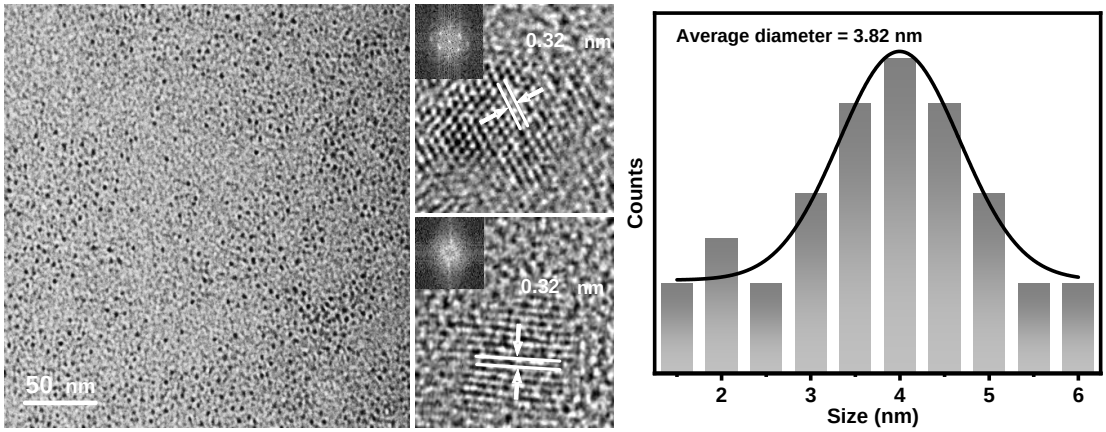

Fig. 1. Morphology of N, B-CQDs: TEM, HRTEM images and size distribution diagram.

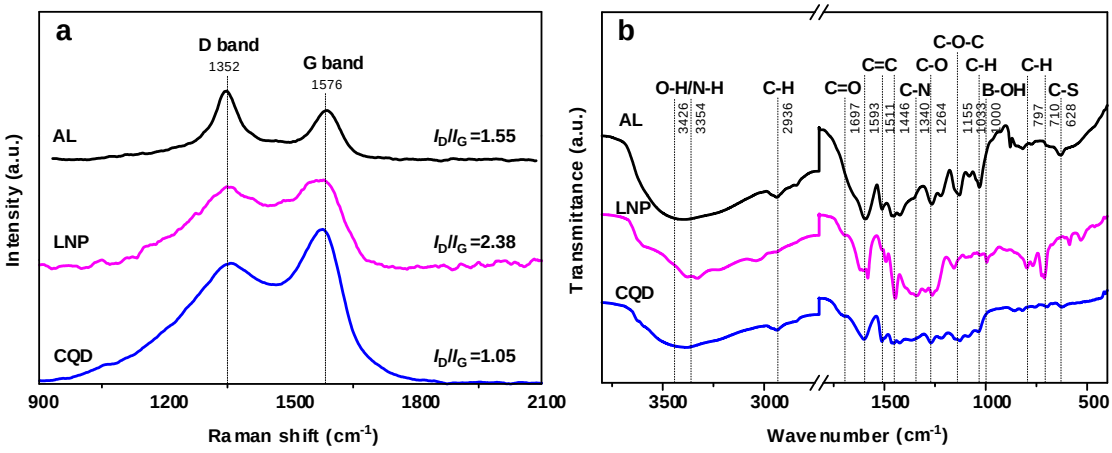

Fig. 2. Structure characterization: (a) Raman spectra, (b) FTIR spectra of AL，LNP and CQD.

The chemical compositions and functional groups of AL, LNP and CQD are identified by FT-IR and XPS. As depicted in Fig. 2b, the strong peaks at 3426 cm^{-1} in FT-IR spectra are assigned to phenolic hydroxyl group [24], where the stretching vibration is significantly decreased from AL to CQD. The peaks located at 2936 and 1033 cm^{-1} are corresponding to in-plane and out-of-plane bending of aromatic C-H [25]. The peaks at 1697, 1511/1593, 1264 and 1155 cm^{-1} are ascribed to C=O, aromatic C=C, C-O and C-O-C stretching vibration, respectively [26]. Notably, the ether vibration (C-O-C) from AL gradually disappears in LNP and CQD, while the new stretching peaks of N-H, C-N and B-OH groups are emerged at 3354, 1340 and 1000 cm^{-1} in LNP and CQD [18, 27]. These demonstrate that CQD inherits the aromatic skeletons from AL and derives the N, B co-doping from LNP by acid hydrolysis of AL. Meanwhile, plentiful polar functional groups (-OH, N-H, C=O, C-O, and B-OH) attached at the edge of the aromatic skeletons of CQD suggest its outstanding hydrophilicity [14, 21, 28]. These results can be further confirmed by XPS analysis. The XPS survey spectra in Fig.3a, f and k show prominent peaks at 168.0, 190.1 284.8, 399.1, and 532.1 eV, which assigned to S2p, B1s, C1s, N1s, and O1s, respectively[15, 18, 23, 29]. AL is mainly composed of C and O along with a small amount of N and S, while LNP and CQD have similar components of C, O, N and B. The high-resolution XPS spectra of C1s, O1s, N1s, and B1s are displayed in Fig. 4b-o. The C1s spectra can be fitted with three peaks at 284.8, 286.2, and 288.2 eV, corresponding to sp^2 carbon (C-C/C=C), sp^3 carbon (C-O/C-N), and carbonyl groups (C=O) [30]. There is a sharply decreased C-O peak from AL to CQD. The O1s spectra can be deconvoluted into two peaks at 531.8 and 533.2 eV for C=O and C−O-C/C-OH [31], where the latter is decreased from AL to LNP. This indicates the cleavage of ether bond by the

183 acidolysis of AL. The N1s spectra show two peaks at 399.7 and 401.8 eV for N-H and C-N
184 groups [32]. The S2p spectra present two peaks at 162.2 and 167.8 eV corresponding to C-S
185 and C-SOx groups [22]. The B1s spectra can be deconvoluted into two peaks at 190.6 and
186 192.3 eV corresponding to B-C and B-O groups [32]. Remarkably, there are no significant
187 signals of N1s and B1s of AL, which are consistent with the FT-IR results. The graphitic C-N
188 and C-B units newly appear from LNP to CQD, inferring that doped N and B are inclined to
189 combine at the edge sites of CQD along with a small amount of lattice doping. These findings
190 can be evidently supported by the quantitative results of XPS analysis as listed in Table S1.
191 The C content decreases first and then increases while O content is the opposite, implying the
192 depolymerization of AL followed by the re-fusion of LNP into the aromatic skeletons of CQD
193 during the synthetic process.

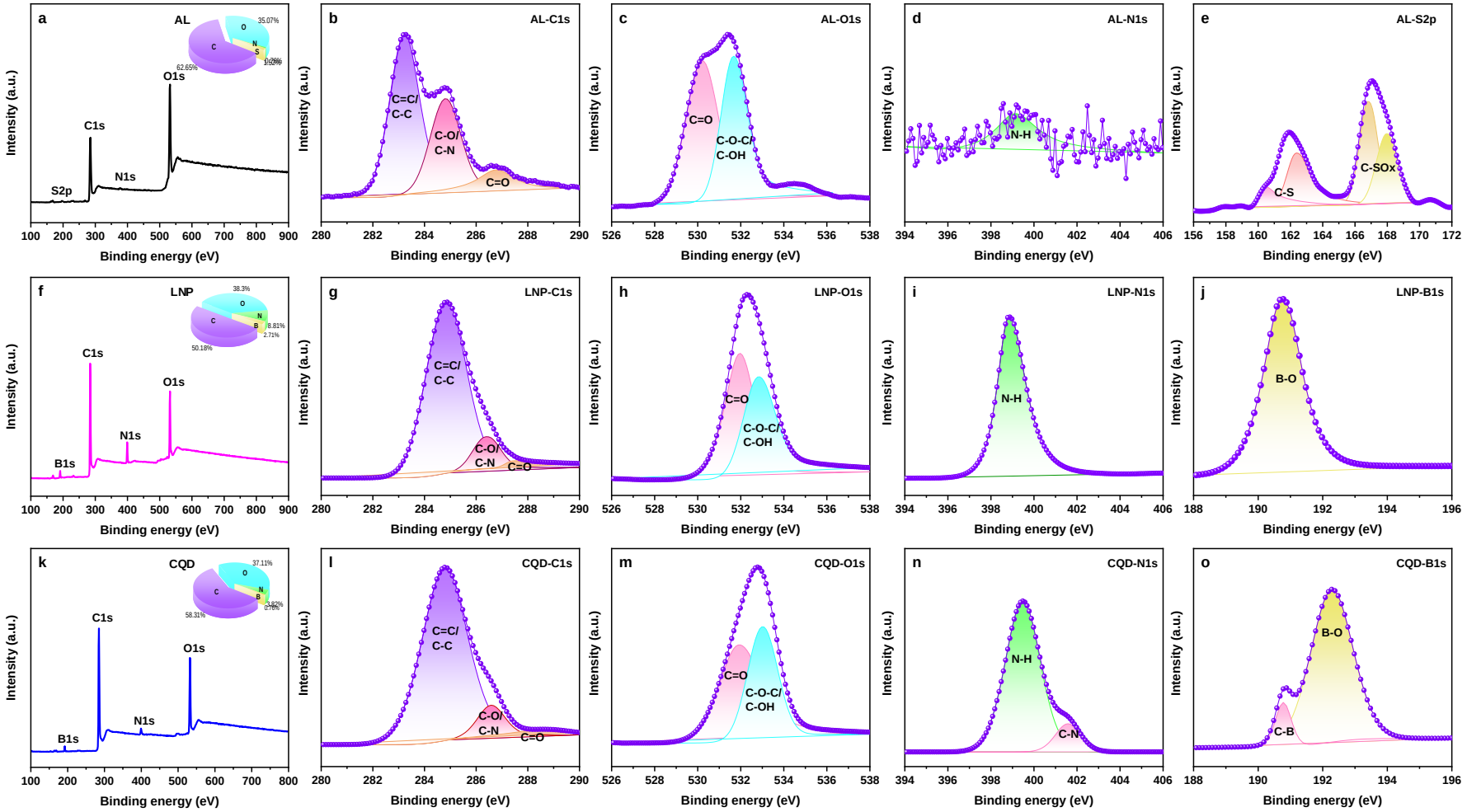

Fig. 3. Structure characterization: (a, f, k) survey and High-resolution (b, g, l) C1s, (c, h, m) O1s, (d, i, n) N1s, (e) S2p and (j, o) B1s XPS spectra of AL, LNP and CQD.

3.2 Formation mechanism of N, B-CQDs

The 2D- HSQC NMR spectra of AL, LNP and CQD are characterized for the in-depth structural insights on the transformation of lignin in the two-step process (Fig. 4). Lignin is an amorphous polymer with a three-dimensional network structure, which is composed of three types of phenylpropane units connected by ether bonds or C-C bonds [33, 34]. The HSQC data of AL show plentiful signals in the side-chain region (δ_C/δ_H: 50–90/3.2–5.0 ppm), assigned to the native structure of lignin including methoxyls (OCH_3), β-aryl-ether linkages (A), phenylcoumarane structures (B) and resinol linkages (C) [35]. The signals of ferulate (FA), p-hydroxyphenyl (H), (G) guaiacyl units and (G') oxidized guaiacyl units are apparently exhbited in the aromatic region (δ_C/δ_H: 100–135/6.0–7.8 ppm) [36, 37]. In comparison, the side-chain signals of A, B and C linkages are sharply reduced in the HSQC data of LNP, and even almost vanish in the HSQC data of CQD, which are in consistent with the above Raman, FT-IR and XPS results. It qualitatively demonstrates that LNP is obtained by strongly de-etherified after the acid treatment of AL via the cleavage of A, B and C linkages. Meanwhile, the N and B dual-doping evidenced by FT-IR and XPS results may contribute to abundant active sites exposed on the surface of LNP for further transformation. The aromatic structures (FA, H, G and G') of AL are well inherited by LNP and CQD in the synthesis process.

According to the experimental evidences above, the formation mechanism of N,B-CQDs from AL via the two-step route is proposed as follows (Fig. 5): In the 1st step of acid hydrolysis, AL is de-ether decomposed into lignin fragments (LNP) through the catalytic cleavage of ether linkages, with simultaneous N, B co-doping via convalent conjugation [28].

Thereby, various active sites including oxygen-, nitrogen- and boron- functional groups can be generate on the LNP surface. 3-Aminophenylboronic acid plays a triple role of "top-down" scissor, N,B dopant as well as surfactant during the acidolysis process [14, 38]. In the 2nd step, the functionalized LNP serves as precursors for the preparation of CQD. The dehydration condensation of activated side chains on LNP result in the prompt π-π stacking and the increased sp^2 hybridization under the hydrothermal treatment [22, 39]. The C–N and C–B groups are simultaneously enhanced in the carbonization process, eventually resulting in the formation of CQD [40]. In summary, the formation of N,B co-doped CQDs involves the acid dissociation of AL first followed by the aromatic re-fusion of LNP.

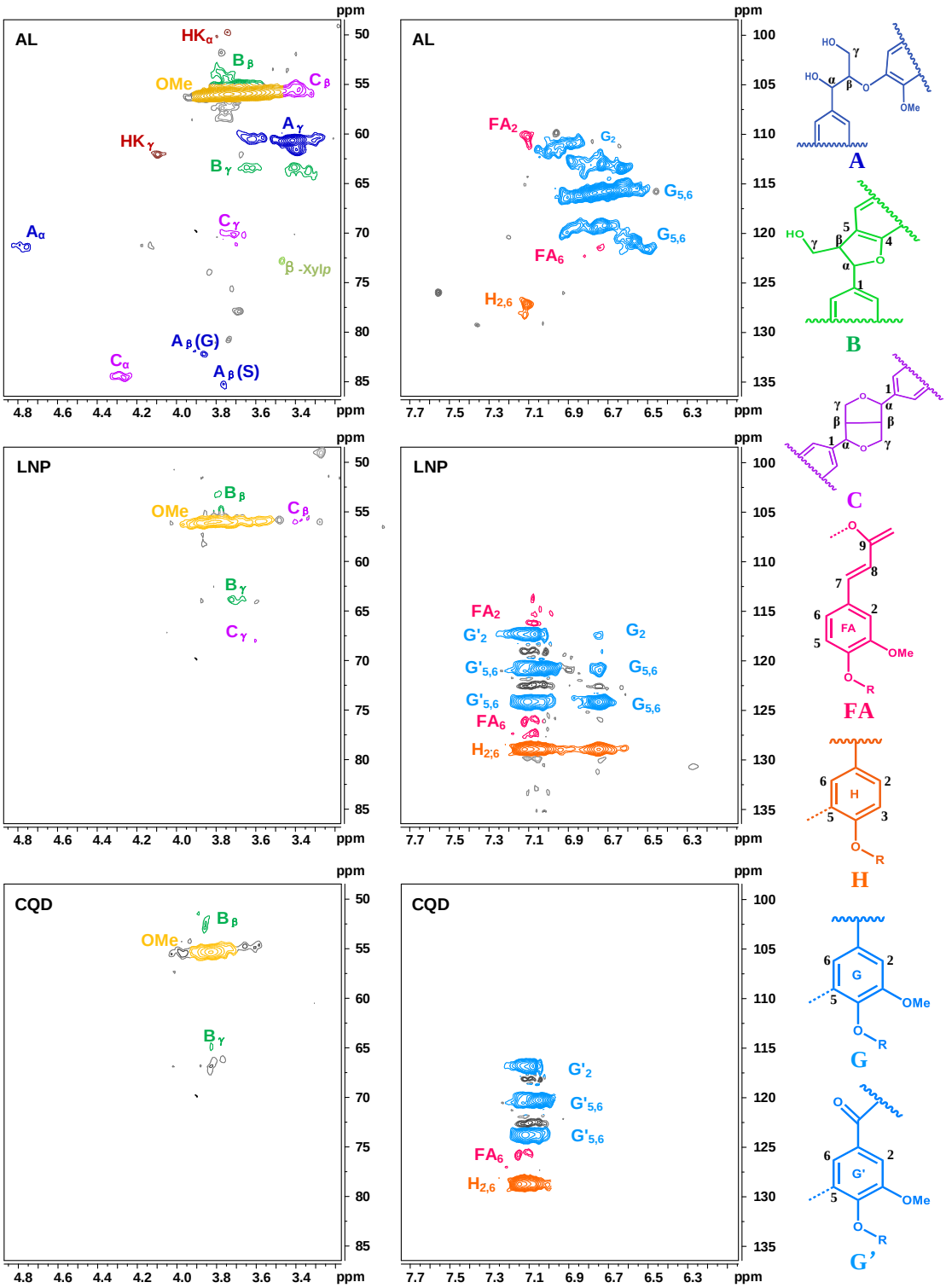

Fig. 4. Main substructures identified in the 2D- HSQC NMR spectra of AL, LNP and CQD: (A) β-O-4’ linkages; (B) phenylcoumaran with α-O-4’ and β-O-5’ linkages; (C) resinol with β–β’, α-O-γ’, and γ-O-α’ linkages; (FA) ferulate; (H) p-hydroxyphenyl; (G) guaiacyl units and (G’) oxidized guaiacyl unit bearing a carbonyl group at Cα.

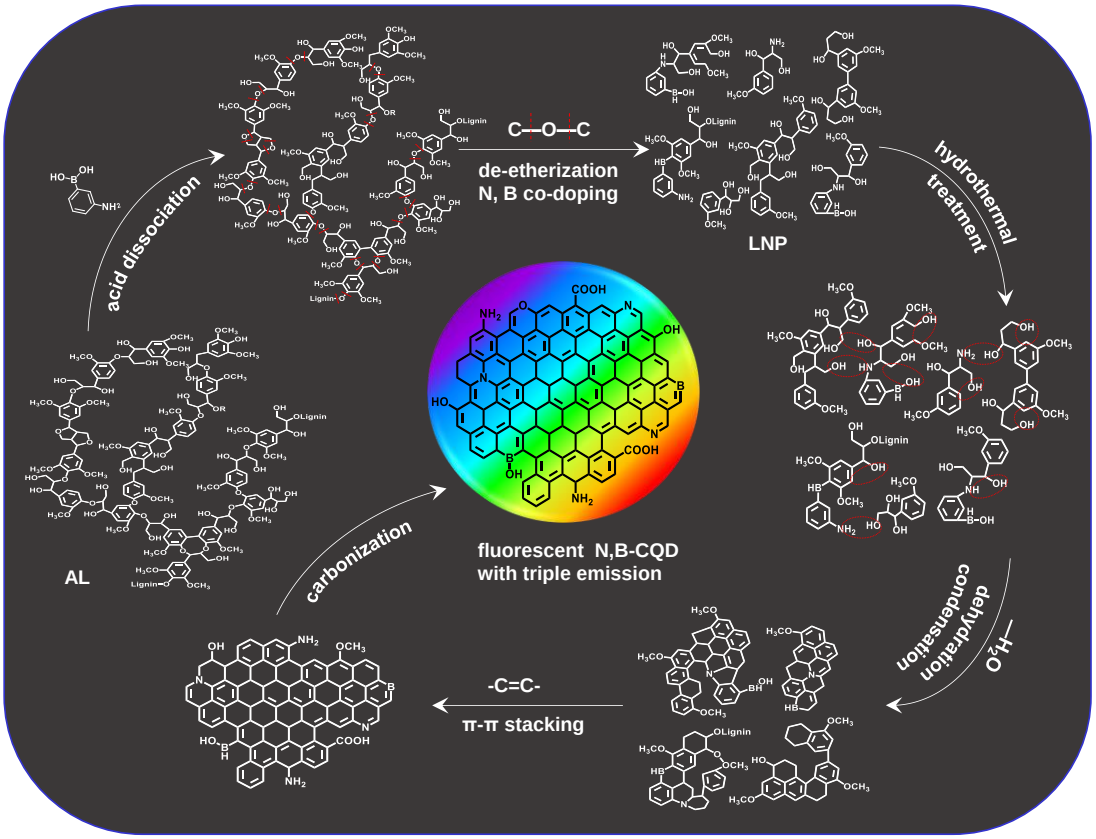

Fig. 5. Proposed formation mechanism of N,B-CQDs from AL via two-step route.

3.3 Optical properties of fluorescent N, B-CQDs

The optical properties of fluorescent N,B-CQDs are further investigated. The PL emission spectra under different excitation wavelengths of 200-700 nm are displayed in Fig. 6a-b. There are three distinct PL centers located at (300, 346), (330, 428), and (490, 514) nm, corresponding to the fluorescence emission of purple, blue and green color, respectively. This indicates that the N,B-CQDs prepared from AL have unique triple-fluorescence emission, which is rarely found in the previous reported biomass-derived CQDs [41, 42]. In detail, N,B-CQDs exhibit almost excitation-independent property under the excitation of 230-300 nm and 440-490 (Fig. S2a, c). Oppositely, the emission peaks are gradually red-shifted from 350 to 496 nm when the excitation wavelengths increase from 310 to 430 nm with a 10 nm

increment (Fig. S2b). This pronounced excitation-dependent behavior is associated with diverse surface defects introduced by O, N or B functional groups [32, 38]. As for the UV-vis absorption spectra (Fig. 6c), N,B-CQDs show two strong adsorption peaks at 230, 281 nm and a weak one at 343 nm, with an optical adsorption edge at ~500 nm. The first two peaks below 300 nm are attributed to the π–π* transition of C=C in the carbon core, while the other are corresponding to the n–π* transition of C=O/C=N on the surface of CQDs [43, 44]. Their corresponding absorbance intensity depends on the conjugated degree in the carbon core and defects state on the surface, respectively.

As shown in Fig. 6d, the TRPL spectra of the triple-emission N,B-CQDs are monitored at $\lambda_{ex}/\lambda_{em}$ of 300/346, 330/428 and 490/514 nm, respectively. The three decay curves can be bioexponentially fitted at the excitation of 300 and 330 nm while monoexponentially fitted at 490 nm (the fitting parameters are summarized in Table S2). The τ_{avg} of N,B-CQDs at 300, 330 and 490 nm excitation are 1.26, 3.91 and 3.41 ns, respectively, which are consistent with the variation trend of QYs. The bioexponential lifetimes denote two PL centers including a fast component (τ_1) originated from the radiative recombination of intrinsic state (π-π*) as well as a slow component (τ_2) ascribed to the non-radiative process of surface state (n-π*) [29, 45]. The percentages of τ_1 excited at 300 and 330 nm of the N,B-CQDs are 81.55% and 75.93%, which demonstrate that their PL emissions are mainly attributed to the sp^2 conjugated structure in the carbon core. The percentage of τ_2 excited at 330 nm increases to 24.07% compared with that at 300 nm, corresponding to the enhanced effect of surface defects on PL emission. The PL emissions of N,B-CQDs excited at 490 nm present a monoexponential lifetime, implying a single PL center of molecular state [46, 47]. The difference concerning

PL centers at 300, 330 and 490 nm excitation further explains the triple-emission performance of N,B-CQDs. As well known, the O, N and B-related functional groups may serve as electron acceptor and surface-passivation agent to induce strong intramolecular charge transfer and improved emission efficiency, respectively. The O-related functional groups, especially C=O with strong electron-accepting property are considered to be chromophores. The N, B related groups are identified as auxochrome groups, the isolated n electrons of which and π electrons of the carbon ring are almost coplanar. The generated defect states lead to the additional energy levels (n-π* transitions) between π and π* transition [48]. The additional n-π* transitions result in multiple radiation recombination paths back to the ground state, thereby exhibiting unique PL performances [49]. In general, the triple-emission behavior of N,B-CQDs depends on the comprehensive effect of carbon core and surface defect state.

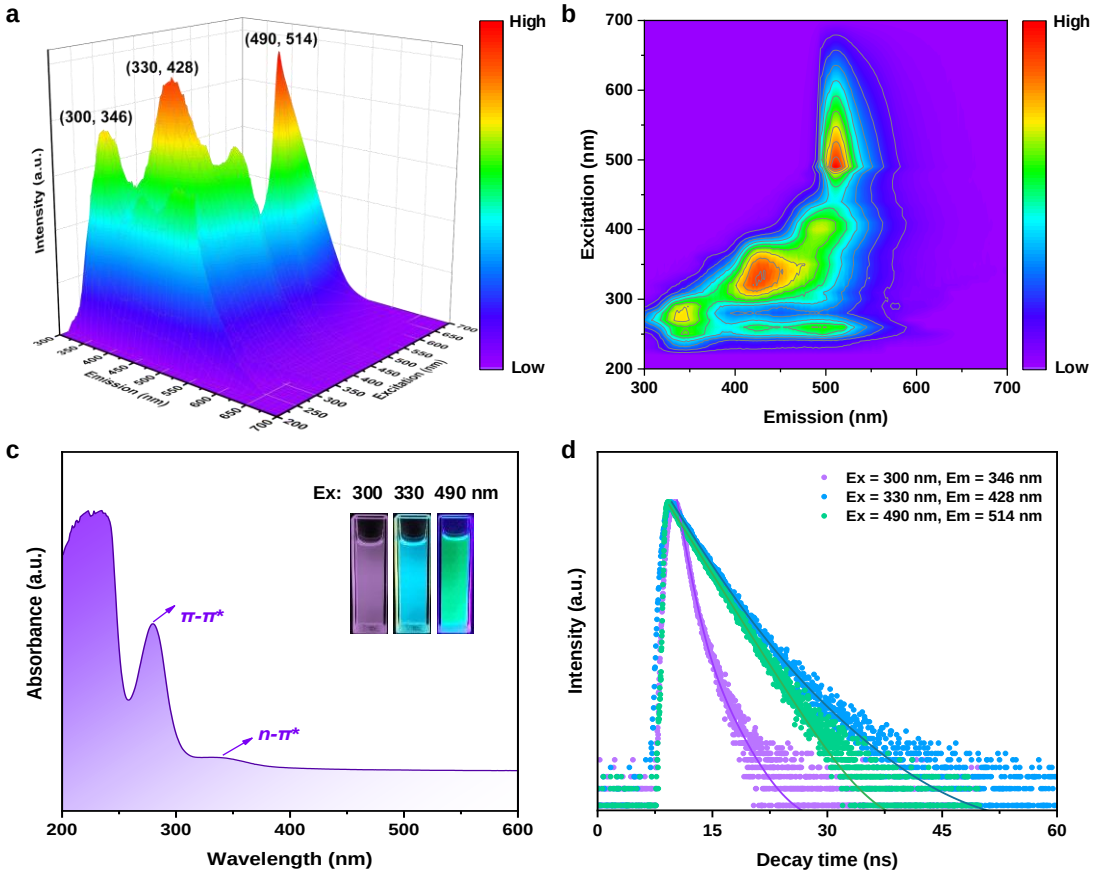

Fig. 6. Optical properties of N,B-CQDs: (a) Three-dimensional (3D) fluorescence spectra, (b) Detailed PL emission spectra under different excitation wavelengths in the range from 200 to 700 nm, (c) UV-vis absorption spectra, inset: photographs of N,B-CQD aqueous solution under different excitation lights (300, 330 and 490 nm), (d) TRPL decay curves at emission of 346, 428, and 514 nm with the fitted curves.

3.4 Tri-channel sensitive detection of Cr^{6+}

Based on the green synthesis, low toxicity, good water solubility and unique optical properties, the selective and sensitive detection for Cr^{6+} is investigated to estimate performance of N, B-CQDs-based fluorescent sensor. The selectivity of N,B-CQDs towards Cr^{6+} and other interfering ions is evaluated, including the anions of Cl^-, F^-, S^{2-}, NO_3^-, SO_3^{2-}, SO_4^{2-}, $H_2PO_2^-$ and metal cations of Na^+, K^+, Ni^{2+}, Mg^{2+}, Cu^{2+}, Ca^{2+}, Zn^{2+}, Fe^{3+}, and Cr^{6+}. As

presented in Fig.7a-c, the PL intensity of N,B-CQDs aqueous solution is maintained well in the presence of different interfering ions (600 μM). However, there is a significant fluorescence quenching in terms of Cr^{6+} under 300, 330 and 490 nm excitation, respectively. Comparing to other CQD-based sensors that also have a fluorescence quenching effect on Fe^{3+}, this N,B-CQDs-based sensor exhibit the superiority in selectivity. The Cr^{6+} induced fluorescence quenching is considered to be originated from the dynamic quenching dominated by collisional deactivation [5, 15, 17, 18]. UV-Vis spectra of Cr^{6+}, N,B-CQDs and N,B-CQDs in the presence of Cr^{6+} are shown in Fig. S3. There are two strong absorption peaks around 270 and 368 nm, which are overlapped with those of N,B-CQDs. It may suppress electron transitions and cause extinction effect on the fluorescence emission of N,B-CQDs [10]. In addition, N,B-CQDs are decorated with $–NH_2$, -COOH and –OH surface groups as electron donors, and Cr^{6+} has stronger binding affinity than other interfering ions towards the electron-donating groups. It can induce considerable energy dissipation instead by rapider electron transfer and restrain recombination of excitons, thereby sharper fluorescence reduction of N,B-CQDs [14, 18].

The sensitivity of N,B-CQDs for Cr^{6+} detection is tested within a wide concentration range of Cr^{6+} from 0 to 1000 μM. As displayed in Fig. d-f, the PL intensity gradually decrease with the increase of the Cr^{6+} concentration, implying the high sensitivity of the concentration dependent fluorescence quenching. It is worth noting that this phenomenon is simultaneously occurred under 300, 330 and 490 nm excitation, demonstrating the feasibility of N,B-CQDs as a tri-channel detection of Cr^{6+}. The linear correlation coefficients (R^2) at concentration range of 0-1000 μM are observed as 0.968, 0.994 and 0.954 for Ex 300, 330 and 490 nm

channel, respectively in Fig. g-i. Furthermore, the higher R^2 are obtained as 0.993, 0.992 and 0.996 at a narrow concentration range of 0-100 μM. Accordingly, the LOD can reach as low as 0.054, 0.049 and 0.077 μM, respectively, which are far lower than the maximum level of drinking water (0.962 μM) permitted by the World Health Organization (WHO) [1]. The lignin-derived N,B-CQDs are comparable to most previously reported CQDs for Cr^{6+} detection regarding the LOD and linear range (Table 1). These results demonstrate that comparable accuracy is achieved for N,B-CQDs based fluorescent sensor, especially the Ex 330 nm channel. Therefore, N,B-CQDs have great potential in the tri-channel detection of Cr^{6+} in practical application.

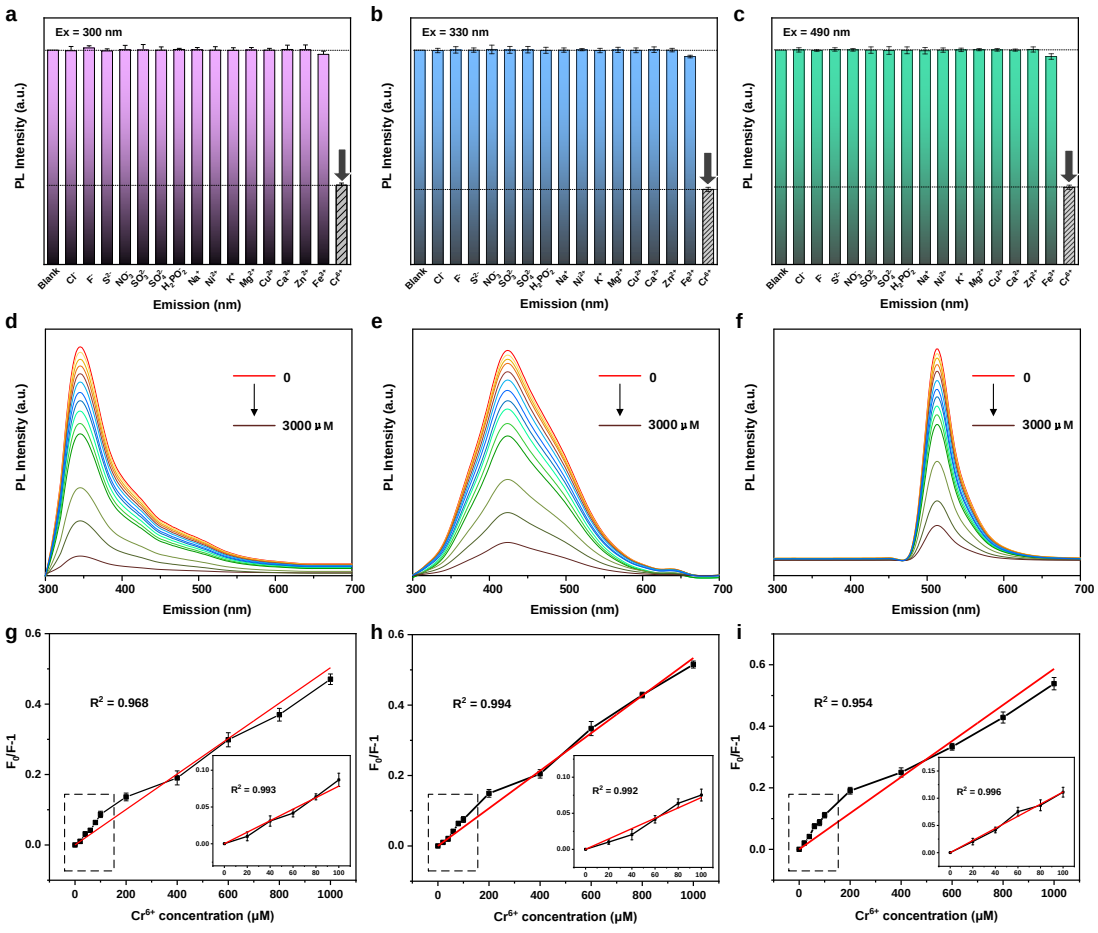

Fig. 7. (a-c) The fluorescence responses of N,B-CQDs with the addition of various interfering ions (600 μM); (d-f) the fluorescence spectra of N,B-CQDs in the presence of

different concentration of Cr^{6+} (0-1000 μM); (g-i) the linear fitting curves of $(F_0-F)/F_0$ at the different concentrations of Cr^{6+} in the range of 0-1000 mM and 0-100 (insert) excited under 300, 330 and 490 nm, respectively.

Table 1. Highly sensitive Cr^{6+} detection of N,B-CQDs compared with other reported CQDs, based on the responsive fluorescence quenching.

Fluorescent sensors	Performances		References
	Limit of detection (μM)	Linear range (μM)	
Cysm-CQDs	1.570	1-10	[50]
CQDs	0.160	2-80	[51]
N,B-CQDs	0.41	0-100	[18]
af-CQDs	0.242	0.8-80	[17]
N-CQDs	0.260	0-12	[10]
S,N-CDs/PVA film	0.093	0.1–50	[12]
Co-CQDs	1.17	5 -125	[52]
N,B-CQDs	0.054	0-100	This work
N,B-CQDs	0.049	0-100	This work
N,B-CQDs	0.077	0-100	This work

4. Conclusions

The fluorescent N,B co-doped CQDs from renewable lignin waste are fabricated by a green two-step strategy to develop a versatile sensitive platform for detection of Cr^{6+} ions. The formation mechanism of N,B co-doped CQDs involves the de-etherization and depolymerization of AL in the acidolysis step, followed by the aromatic re-fusion of LNP in the hydrothermal treatment. The resultant N,B-CQDs exhibit triple fluorescent emission under the excitation of 300, 330, and 90 nm, which are considered to be induced by the synergistic effect of carbon core state and surface defect state. The triple-emission N,B-CQDs are utilized for the highly selective and sensitive detection of Cr^{6+} with the LOD as low as 0.144, 0.082

and 0.094 μM in Ex 300, 330 and 490 nm channel, respectively. The sensing mechanism may be attributed to the decorated electron-donating amino, carboxyl, hydroxyl groups on the CQD surface, which combine Cr^{6+} to cause the dynamic fluorescence quenching. The fluorescence sensing platform based on N,B-CQDs is constructed, which provides new insights on the rapid, visualized and accurate detection of Cr^{6+} through triple channel in aqueous media.

CRediT authorship contribution statement

Lingli Zhu: Investigation, Methodology, Data curation, Writing-original draft, Validation. Dekui Shen: Conceptualization, Investigation, Writing-original draft, Funding acquisition. Kai Hong Luo: Writing-review, Supervision.

Declaration of Competing Interest

The authors declare that they have no known competing financial interests or personal relationships that could have appeared to influence the work reported in this paper.

Acknowledgements

The authors gratefully acknowledge the financial support from National Natural Science Foundation of China (grant numbers. 51676047 and 51861145102) and the Key Research & Development Program of Jiangsu Province (grant number: BE2020114). The authors also acknowledge the funding support from the Scientific Research Foundation of Graduate School of Southeast University, China (YBPY2109) and Postgraduate Research & Practice Innovation Program of Jiangsu Province from the Education Department of Jiangsu (KYCX21_0094).

Appendix A. Supplementary data

Supplementary material related to this article can be found, in the online version, at

References

[1] Y. Mao, S. Gao, L. Yao, L. Wang, H. Qu, Y. Wu, Y. Chen, L. Zheng, Single-atom nanozyme enabled fast and highly sensitive colorimetric detection of Cr(VI), J Hazard Mater, 408 (2021) 124898.

[2] S. Li, T. Wei, G. Ren, F. Chai, H. Wu, F. Qu, Gold nanoparticles based colorimetric probe for Cr(III) and Cr(VI) detection, Colloids and Surfaces A: Physicochemical and Engineering Aspects, 535 (2017) 215-224.

[3] S. Shahim, R. Sukesan, I. Sarangadharan, Y.L. Wang, Multiplexed Ultra-Sensitive Detection of Cr(III) and Cr(VI) Ion by FET Sensor Array in a Liquid Medium, Sensors (Basel), 19 (2019).

[4] O. Dvoynenko, S.L. Lo, Y.J. Chen, G.W. Chen, H.M. Tsai, Y.L. Wang, J.K. Wang, Speciation Analysis of Cr(VI) and Cr(III) in Water with Surface-Enhanced Raman Spectroscopy, ACS Omega, 6 (2021) 2052-2059.

[5] Y. Wang, X. Hu, W. Li, X. Huang, Z. Li, W. Zhang, X. Zhang, X. Zou, J. Shi, Preparation of boron nitrogen co-doped carbon quantum dots for rapid detection of Cr(VI), Spectrochimica Acta Part a-Molecular and Biomolecular Spectroscopy, 243 (2020).

[6] J. Wang, Z. Wu, S. Chen, R. Yuan, L. Dong, A novel multifunctional fluorescent sensor based on N/S co-doped carbon dots for detecting Cr (VI) and toluene, Microchemical Journal, 151 (2019).

[7] Y. Yang, X. Chen, Y. Wang, M. Wu, Y. Ma, X. Yang, A Novel Fluorescent Test Papers Based on Carbon Dots for Selective and Sensitive Detection of Cr (VI), Front Chem, 8 (2020) 595628.

[8] A. Tall, F. Antônio Cunha, B. Kaboré, C. d'Angeles do E. S. Barbosa, U. Rocha, T.O. Sales, M.O. Fonseca Goulart, I. Tapsoba, J. Carinhanha Caldas Santos, Green emitting N, P-doped carbon dots as efficient fluorescent nanoprobes for determination of Cr(VI) in water and soil samples, Microchemical Journal, 166 (2021).

[9] X. Luo, P. Bai, X. Wang, G. Zhao, J. Feng, H. Ren, Preparation of nitrogen-doped carbon quantum dots and its application as a fluorescent probe for Cr(vi) ion detection, New Journal of Chemistry, 43 (2019) 5488-5494.

[10] S. Liu, J. Cui, J. Huang, B. Tian, F. Jia, Z. Wang, Facile one-pot synthesis of highly fluorescent nitrogen-doped carbon dots by mild hydrothermal method and their applications in detection of Cr(VI) ions, Spectrochim Acta A Mol Biomol Spectrosc, 206 (2019) 65-71.

[11] B. Li, H. Ma, B. Zhang, J. Qian, T. Cao, H. Feng, W. Li, Y. Dong, W. Qin, Dually emitting carbon dots as fluorescent probes for ratiometric fluorescent sensing of pH values, mercury(II), chloride and Cr(VI) via different mechanisms, Mikrochim Acta, 186 (2019) 341.

[12] Y. Ji, X. Zou, W. Wang, T. Wang, S. Zhang, Z. Gong, Co-Doped S, N-Carbon dots and its

fluorescent film sensors for rapid detection of Cr (VI) and Ascorbic acid, Microchemical Journal, 167 (2021).
[13] A.K. Singh, V.K. Singh, M. Singh, P. Singh, S.R. Khadim, U. Singh, B. Koch, S.H. Hasan, R.K. Asthana, One pot hydrothermal synthesis of fluorescent NP-carbon dots derived from Dunaliella salina biomass and its application in on-off sensing of Hg (II), Cr (VI) and live cell imaging, Journal of Photochemistry and Photobiology a-Chemistry, 376 (2019) 63-72.
[14] R. Wang, L. Jiao, X. Zhou, Z. Guo, H. Bian, H. Dai, Highly fluorescent graphene quantum dots from biorefinery waste for tri-channel sensitive detection of Fe3+ ions, Journal of hazardous materials, 412 (2021) 125096-125096.
[15] J. Shen, S. Shang, X. Chen, D. Wang, Y. Cai, Highly fluorescent N, S-co-doped carbon dots and their potential applications as antioxidants and sensitive probes for Cr (VI) detection, Sensors and Actuators B: Chemical, 248 (2017) 92-100.
[16] S. Chaudhary, S. Kumar, B. Kaur, S.K. Mehta, Potential prospects for carbon dots as a fluorescence sensing probe for metal ions, Rsc Advances, 6 (2016) 90526-90536.
[17] X. Zheng, S. Ren, L. Wang, Q. Gai, Q. Dong, W. Liu, Controllable functionalization of carbon dots as fluorescent sensors for independent Cr(Ⅵ), Fe(Ⅲ) and Cu(Ⅱ) ions detection, Journal of Photochemistry and Photobiology A: Chemistry, 417 (2021).
[18] M. Jia, L. Peng, M. Yang, H. Wei, M. Zhang, Y. Wang, Carbon dots with dual emission: A versatile sensing platform for rapid assay of Cr (VI), Carbon, 182 (2021) 42-50.
[19] F. Li, Y. Li, X. Yang, X. Han, Y. Jiao, T. Wei, D. Yang, H. Xu, G. Nie, Highly Fluorescent Chiral N-S-Doped Carbon Dots from Cysteine: Affecting Cellular Energy Metabolism, Angewandte Chemie-International Edition, 57 (2018) 2377-2382.
[20] H. Zhang, S. Kang, G. Wang, Y. Zhang, H. Zhaou, Fluorescence Determination of Nitrite in Water Using Prawn-Shell Derived Nitrogen-Doped Carbon Nanodots as Fluorophores, Acs Sensors, 1 (2016) 875-881.
[21] B. Zhang, Y. Liu, M. Ren, W. Li, X. Zhang, R. Vajtai, P.M. Ajayan, J.M. Tour, L. Wang, Sustainable Synthesis of Bright Green Fluorescent Nitrogen-Doped Carbon Quantum Dots from Alkali Lignin, Chemsuschem, 12 (2019) 4202-4210.
[22] L. Zhu, D. Shen, Q. Liu, C. Wu, S. Gu, Sustainable synthesis of bright green fluorescent carbon quantum dots from lignin for highly sensitive detection of Fe3+ ions, Applied Surface Science, 565 (2021).
[23] Y. Liu, H. Yang, C. Ma, S. Luo, M. Xu, Z. Wu, W. Li, S. Liu, Luminescent Transparent Wood Based on Lignin-Derived Carbon Dots as a Building Material for Dual-Channel, Real-Time, and Visual Detection of Formaldehyde Gas, ACS Appl Mater Interfaces, 12 (2020) 36628-36638.
[24] Y. Zhao, C. Ou, J. Yu, Y. Zhang, H. Song, Y. Zhai, Z. Tang, S. Lu, Facile Synthesis of Water-Stable Multicolor Carbonized Polymer Dots from a Single Unconjugated Glucose for Engineering White Light-Emitting Diodes with a High Color Rendering Index, ACS Appl Mater Interfaces, (2021).
[25] H. Zhao, X. Yu, C.-F. Li, W. Yu, A. Wang, Z.-Y. Hu, S. Larter, Y. Li, M. Golam Kibria, J. Hu, Carbon quantum dots modified TiO2 composites for hydrogen production and selective glucose photoreforming, Journal of Energy Chemistry, 64 (2022) 201-208.
[26] J. Zhang, Y. Lin, S. Wu, X. Hou, C. Zheng, P. Wu, J. Liu, Self-photo-oxidation for

extending visible light absorption of carbon dots and oxidase-like activity, Carbon, 182 (2021) 537-544.
[27] J. Wang, Q. Li, J. Zheng, Y. Yang, X. Liu, B. Xu, N, B-Codoping Induces High-Efficiency Solid-State Fluorescence and Dual Emission of Yellow/Orange Carbon Dots, ACS Sustainable Chemistry & Engineering, 9 (2021) 2224-2236.
[28] R. Wang, G. Xia, W. Zhong, L. Chen, L. Chen, Y. Wang, Y. Min, K. Li, Direct transformation of lignin into fluorescence-switchable graphene quantum dots and their application in ultrasensitive profiling of a physiological oxidant, Green Chemistry, 21 (2019) 3343-3352.
[29] Q. Su, X. Yang, Promoting Room Temperature Phosphorescence through Electron Transfer from Carbon Dots to Promethazine, ACS Appl Mater Interfaces, 13 (2021) 41238-41248.
[30] J. Li, H. Zhao, X. Zhao, X. Gong, Red and yellow emissive carbon dots integrated tandem luminescent solar concentrators with significantly improved efficiency, Nanoscale, 13 (2021) 9561-9569.
[31] W. Chang, B. Ning, Q. Xu, H. Jiang, Y. Hu, C. Li, Strongly coupled N-doped graphene quantum dots/Ni(Fe)OxHy electrocatalysts with accelerated reaction kinetics for water oxidation, Chemical Engineering Journal, (2021).
[32] L. Zhu, D. Shen, Q. Wang, K.H. Luo, Green Synthesis of Tunable Fluorescent Carbon Quantum Dots from Lignin and Their Application in Anti-Counterfeit Printing, ACS Applied Materials & Interfaces, (2021).
[33] C. Zhu, X. Dou, W. Li, X. Liu, Q. Li, J. Ma, Q. Liu, L. Ma, Efficient depolymerization of Kraft lignin to liquid fuels over an amorphous titanium-zirconium mixed oxide supported partially reduced nickel-cobalt catalyst, Bioresour Technol, 284 (2019) 293-301.
[34] J. Zhu, F. Chen, Z. Zhang, M. Li, Q. Yang, Y. Yang, Z. Bao, Q. Ren, M-Gallate (M = Ni, Co) Metal–Organic Framework-Derived Ni/C and Bimetallic Ni–Co/C Catalysts for Lignin Conversion into Monophenols, ACS Sustainable Chemistry & Engineering, 7 (2019) 12955-12963.
[35] H. Luo, M.M. Abu-Omar, Lignin extraction and catalytic upgrading from genetically modified poplar, Green Chemistry, 20 (2018) 745-753.
[36] W. Zhao, L.-P. Xiao, G. Song, R.-C. Sun, L. He, S. Singh, B.A. Simmons, G. Cheng, From lignin subunits to aggregates: insights into lignin solubilization, Green Chemistry, 19 (2017) 3272-3281.
[37] M. Wang, J. Lu, X. Zhang, L. Li, H. Li, N. Luo, F. Wang, Two-Step, Catalytic C–C Bond Oxidative Cleavage Process Converts Lignin Models and Extracts to Aromatic Acids, ACS Catalysis, 6 (2016) 6086-6090.
[38] Z. Ding, F. Li, J. Wen, X. Wang, R. Sun, Gram-scale synthesis of single-crystalline graphene quantum dots derived from lignin biomass, Green Chemistry, 20 (2018) 1383-1390.
[39] M. Si, J. Zhang, Y. He, Z. Yang, X. Yan, M. Liu, S. Zhuo, S. Wang, X. Min, C. Gao, L. Chai, Y. Shi, Synchronous and rapid preparation of lignin nanoparticles and carbon quantum dots from natural lignocellulose, Green Chemistry, 20 (2018) 3414-3419.
[40] S. Jing, Y. Zhao, R.-C. Sun, L. Zhong, X. Peng, Facile and High-Yield Synthesis of

Carbon Quantum Dots from Biomass-Derived Carbons at Mild Condition, Acs Sustainable Chemistry & Engineering, 7 (2019) 7833-7843.
[41] A. Abbas, L.T. Mariana, A.N. Phan, Biomass-waste derived graphene quantum dots and their applications, Carbon, 140 (2018) 77-99.
[42] L. Zhu, D. Shen, C. Wu, S. Gu, State-of-the-Art on the Preparation, Modification, and Application of Biomass-Derived Carbon Quantum Dots, Industrial & Engineering Chemistry Research, 59 (2020) 22017-22039.
[43] Y. Zheng, K. Arkin, J. Hao, S. Zhang, W. Guan, L. Wang, Y. Guo, Q. Shang, Multicolor Carbon Dots Prepared by Single- Factor Control of Graphitization and Surface Oxidation for High- Quality White Light- Emitting Diodes, Advanced Optical Materials, (2021).
[44] B. Wang, H. Song, Z. Tang, B. Yang, S. Lu, Ethanol-derived white emissive carbon dots: the formation process investigation and multi-color/white LEDs preparation, Nano Research, (2021).
[45] H. Li, S. Han, B. Lyu, T. Hong, S. Zhi, L. Xu, F. Xue, L. Sai, J. Yang, X. Wang, B. He, Tunable light emission from carbon dots by controlling surface defects, Chinese Chemical Letters, (2021).
[46] T. Zhang, J. Zhu, Y. Zhai, H. Wang, X. Bai, B. Dong, H. Wang, H. Song, A novel mechanism for red emission carbon dots: hydrogen bond dominated molecular states emission, Nanoscale, 9 (2017) 13042-13051.
[47] M. Park, H.S. Kim, H. Yoon, J. Kim, S. Lee, S. Yoo, S. Jeon, Controllable Singlet-Triplet Energy Splitting of Graphene Quantum Dots through Oxidation: From Phosphorescence to TADF, Adv Mater, 32 (2020) e2000936.
[48] X. Li, S.P. Lau, L. Tang, R. Ji, P. Yang, Sulphur doping: a facile approach to tune the electronic structure and optical properties of graphene quantum dots, Nanoscale, 6 (2014) 5323-5328.
[49] Y. Chen, H. Lian, Y. Wei, X. He, Y. Chen, B. Wang, Q. Zeng, J. Lin, Concentration-induced multi-colored emissions in carbon dots: origination from triple fluorescent centers, Nanoscale, 10 (2018) 6734-6743.
[50] R. V, V. Gujar, H. Pathan, S. Islam, M. Tawre, K. Pardesi, M.K. Santra, D. Ottoor, Bioimaging Applications of Carbon dots (C. dots) and its Cystamine Functionalization for the Sensitive Detection of Cr(VI) in Aqueous Samples, J Fluoresc, 29 (2019) 1381-1392.
[51] Y. Liu, Z. Chen, W. Li, C. Ma, P. Wu, X. Wu, S. Li, S. Liu, A nanocomposite probe consisting of carbon quantum dots and phosphotungstic acid for fluorometric determination of chromate(VI) with improved selectivity, Mikrochim Acta, 185 (2018) 470.
[52] H.-Y. Zhang, Y. Wang, S. Xiao, H. Wang, J.-H. Wang, L. Feng, Rapid detection of Cr(VI) ions based on cobalt(II)-doped carbon dots, Biosensors & Bioelectronics, 87 (2017) 46-52.

Highlights

- Facile two-step route is proposed for synthesizing triple-emission fluorescent N, B-CQDs derived from lignin waste.

- The formation mechanism of N,B-CQDs from lignin-derived via two-step route is deeply excavated.

- The highly fluorescent tri-channel sensing platform based on N,B-CQDs sensor has been established.

Declaration of interests

☒The authors declare that they have no known competing financial interests or personal relationships that could have appeared to influence the work reported in this paper.

☒The authors declare the following financial interests/personal relationships which may be considered as potential competing interests:

Dekui Shen reports financial support was provided by National Natural Science Foundation of China. Dekui Shen reports financial support was provided by Key Research & Development Program of Jiangsu Province. Dekui Shen reports financial support was provided by Postgraduate Research & Practice Innovation Program of Jiangsu Province from the Education Department of Jiangsu.